AIP | The Journal of Chemical Physics

Low temperature phase properties of water confined in mesoporous silica MCM-41: Thermodynamic and neutron scattering study

Shigeharu Kittaka, Shuichi Takahara, Hideyuki Matsumoto, Yasuki Wada, Taku J. Satoh, and Toshio Yamaguchi

Citation: The Journal of Chemical Physics **138**, 204714 (2013); doi: 10.1063/1.4807593
View online: http://dx.doi.org/10.1063/1.4807593
View Table of Contents: http://scitation.aip.org/content/aip/journal/jcp/138/20?ver=pdfcov
Published by the AIP Publishing

Low temperature phase properties of water confined in mesoporous silica MCM-41: Thermodynamic and neutron scattering study

Shigeharu Kittaka,[1,a)] Shuichi Takahara,[1] Hideyuki Matsumoto,[1] Yasuki Wada,[1] Taku J. Satoh,[2] and Toshio Yamaguchi[3,4]
[1]*Department of Chemistry, Faculty of Science, Okayama University of Science, 1-1 Ridaicho, Kita-ku, Okayama 700-0005, Japan*
[2]*Institute of Multidisciplinary Research for Applied Materials, Tohoku University, 2-1-1 Katahira, Sendai 980-8577, Japan*
[3]*Department of Chemistry, Faculty of Science, Fukuoka University, Jonan, Fukuoka 814-0180, Japan*
[4]*Advanced Materials Institute, Fukuoka University, Jonan, Fukuoka 814-0180, Japan*

(Received 5 January 2013; accepted 8 May 2013; published online 31 May 2013)

The phase properties of water confined in mesoporous silica MCM-41 were investigated over a temperature range of 100–298 K as a function of pore size by specific heat capacity and inelastic neutron scattering (INS) measurements. The water content of the samples was carefully controlled to ensure the capillary filled state and no overloading of water. The values of heat capacity of the pore water are higher than those of bulk ice and liquid water over the whole temperature range measured. The contribution of water in the inner part of pores (abbreviated as the internal water) was elucidated by using the heat capacity data of monolayer water measured. The entropy of the internal water was then estimated from integration of the heat capacity of the internal water. The entropy values of the internal water increase by confinement in the pores of MCM-41 in both liquid and frozen regions, indicating an increase in the deformation of the structure and/or a change in the dynamics in both regions. The INS spectra show the density of states for the librational motion of water frozen at 50 K, suggesting that the confined water is similar to amorphous ice rather than to crystalline ice. When the sample is warmed to melt, the band edge of the librational motion for water frozen in large pores (diameter of 3.6 nm) shifts to a lower energy side, indicating the weakening of intermolecular hydrogen bonds. For water in small pores (2.1 nm), on the contrary, the librational band shifts slightly to a higher energy side, suggesting the low density liquid to high density liquid transition (L–L transition) at 225–250 K. A plausible mechanism of the L–L transition of water in confinement is proposed in terms of incomplete growth of homogeneous nucleation of ice due to an interfacial free energy effect to inhibit crystallization of water confined in small pores. © *2013 AIP Publishing LLC*. [http://dx.doi.org/10.1063/1.4807593]

I. INTRODUCTION

Water is an essential material on the Earth and occurs in nature as various forms: vapour, liquid, and solid ice. In particular, water in a confined state or in finite clusters plays a vital role in properties and functions of many systems, such as catalyst, fuel cell, membrane proteins, and aerosol. Thus, many physicochemical studies have been performed on confined water. However, a progress in understanding the behaviour of confined water was slow until the beginning of the 1990s because of a lack of reliable samples with defined pore structures. The development of methods to prepare well-defined mesoporous silica with uniform pore size, such as cylindrical FSM-16 and MCM-41 and cage-like SBA-16, has made a remarkable progress in understanding the properties and functions of pore fluids.[1–7] Another advantage of these materials is the pore size that can be controlled by changing the length of the alkyl chain of surfactants employed for a template of micelles. For example, knowledge about the freezing and melting of confined water,[8–10] phase transitions in supercooled liquid water,[11,12] and the presence of boundary water in porous materials,[13,14] is indebted to these materials.

The crystalline phase of water frozen in pores has been studied by using neutron scattering[15,16] and X-ray diffraction analysis[9,17] and has been found to be mainly ice I_c. Based on an X-ray diffraction analysis of ice formed in pores, Morishige and Uematsu[17] have claimed that ice I_c has a fault stacking structure along the (001) plane of ice I_h. From molecular dynamics simulations, Moore *et al.*[18,19] visualized the coexistence of I_c, I_h, and amorphous phases (or liquid water) for both bulk and water confined in cylindrical pores of 3 nm in diameter. X-ray diffraction measurements on pores with a diameter of 3 nm showed broad peaks corresponding to ice Ic.[9]

Pore water may be divided into internal water and interfacial water adjacent to the pore surface. A recent neutron scattering study has shown that the interfacial water has a rigid structure independent of temperature down to 170 K, whereas the structure of the internal water change with temperature.[20]

To investigate the effect of pore size on the thermodynamic properties of confined water, we have performed differential scanning calorimetry (DSC) studies on the freezing and melting of water confined in the cylindrical pores

a)Author to whom correspondence should be addressed. Electronic mail: kittaka@chem.ous.ac.jp

of MCM-41 and SBA-15.[10] It is found that a linear relationship, i.e., the Gibbs–Thomson (G–T) relation, holds between the melting point and the inverse of effective pore size for pore sizes above 2.6 nm, but deviates from the G–T relation for pore sizes below 2.6 nm. The enthalpy change of melting decreases with decreasing pore size, suggesting an increase in deformation of the structure of the liquid and/or solidified confined water, compared with that of bulk water.[10] Johari[21,22] has proposed that fine crystallite grains are formed when supercooled water is frozen. Oguni *et al.*[23] have measured the glass transition (dH/dt) and heat capacity, C_p, of water confined in MCM-41. They reported that a characteristic glass transition of confined water occurred at around 200 K and also a glass transition and melting at 100–120 K of the interfacial water which interacts with the surface hydroxyls. These results have not yet been substantiated by other methods.

The phase transition of supercooled water confined in MCM-41 was first reported at 225 K by Faraone *et al.*[11] using high resolution quasi-elastic neutron scattering. They proposed a change in the mode of the single particle dynamics of confined water. We have carried out neutron spin echo measurements on heavy water confined in MCM-41 ($d = 2.1$ nm) and found a transition in the relaxation time of collective dynamics of confined water from the Vogel–Fulcher–Tammann (VFT) to the Arrhenius type behaviour at 229 K which is similar to the temperature found in the work by Faraone *et al.*[11,12] The transition has been named as Fragile–Strong (FS), high density liquid (HDL)–low density liquid (LDL), or simply L–L transition. Calorimetrically, a phase change signal has been observed from the exothermic and endothermic DSC peaks from water in the mesopores ($d = 2.4$–2.8 nm) around 235 K when cooled and heated, respectively.[13] The Oguni's group[23,24] has made heat capacity, C_p, measurements of water in MCM-41 with different diameters in the range 1.7–4.2 nm on an adiabatic calorimeter. They observed a peak at 233 K, essentially independent of the pore diameter, although the heat capacity values increased in proportion to the fraction of the internal water molecules within the pores.[23,24] This result is surprising because the phase transition in small pores should be subject to a pore size effect. To the best of our knowledge, there is no clear explanation on this observation, although in a recent paper Ngai *et al.*[25] refuted the idea of L–L transition. The comparative results of the change in dynamics and thermodynamics data at around 230 K for confined water have not yet been rationalized explicitly.

In the present work, we determine the heat capacity of confined water precisely by taking into account the following points to obtain thermodynamic parameter (entropy) of confined water. Recently, we have found that supercooled liquid water in the pores affects the behaviour of boundary water over the porous material to freeze later than the external bulky water.[13] Accordingly, the boundary water, i.e., external water, has to be carefully avoided to investigate the pore water selectively. It is understood that interfacial water bound to the surface silanol groups behaves differently from the inner water in the pore center, although Nagoe *et al.*[24] did not consider this contribution in their C_p analysis. Thus, in the present work, we measure the heat capacity of monolayer (ML) water with which the heat capacity of the internal water in cylindrical pores was evaluated. In addition to the thermodynamic data, the density of states of vibration of water is examined by inelastic neutron scattering (INS) measurements. On the basis of these results, we discuss the role of confinement in the phase changes of water, particularly, on the L–L transition of water in confinement.

II. EXPERIMENTAL

A. Materials

The MCM-41 samples used in this study were similar to those employed in previous works.[10,26] The sample names, Cn, denote the number of carbon atoms in the longest alkyl group of the precursor molecule, $C_nH_{2n+1}(CH_3)_3N^+Br^-$. The pore diameters were determined by nitrogen adsorption at the temperature of liquid nitrogen. Pore size analysis was made on the nitrogen absorption data with the Dollimore-Heals[27] method which is usually employed for cylindrical pores: C10, $d = 2.1$ nm; C12, 2.4 nm; C14, 2.8 nm; C16, 3.2 nm; and C18, 3.6 nm. Arrangement and size of cylindrical pores were observed with a high resolution TEM. The pore size distributions of C10 and C14 are uniform and available in the supplementary material.[50]

B. Measurements

1. Adsorption

Adsorption isotherms were determined gravimetrically on a Rubotherm absorption analyser (Japan BEL), which is connected to a gas dosing system controlled with a PC. The adsorption temperature was controlled to 298.2 ± 0.1 K with a water bath connected with a chiller and heating system.

2. Heat capacity

The heat capacity was measured on a homemade adiabatic calorimeter, similar to a standard-type apparatus.[28] The temperature of the sample cell was measured with a platinum resistance thermometer connected to an AC resistance bridge (Tinsley 5840D). The sample cell was surrounded by a double adiabatic shield, whose temperature was controlled to follow the temperature of the sample cell. The sample cell and adiabatic shield were set in a cryostat equipped with a liquid nitrogen reservoir as a cooling unit. The heat capacity was determined from the relationship $C_p = Q/\Delta T$, where Q and ΔT are the Joule heat supplied to the sample cell and the change in temperature, respectively. The Joule heat was generated by applying 100 mA of electric current at a voltage of approximately 5 V for 2 min, which was varied depending on the temperature of the cell. The precision and accuracy of the heat capacity measurements were 0.034% from the measurement of an empty sample cell and 1.2% as copper as a reference sample, respectively.

MCM-41 samples were fully hydrated by suspending the sample powder in water in a test tube, followed by evacuation so that air in the pores was exchanged with water and left

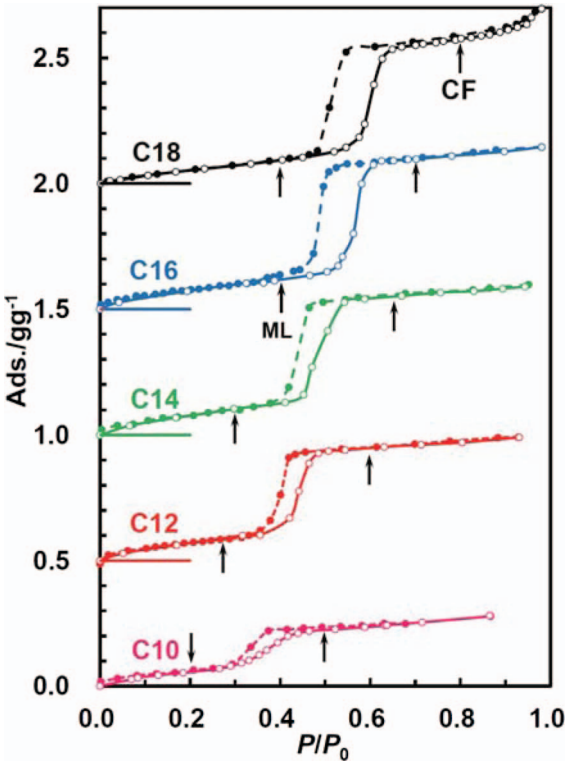

FIG. 1. The adsorption isotherms of water on MCM-41. Each curve is shifted by 0.5 for clarity. The arrows indicate the pressures for monolayer and capillary filling used for the C_p measurements. The adsorbed amounts between the arrows were used to estimate the amount of internal water in the pores. The monolayer values were assigned to the interfacial water and used in the separation of the contributions of the interfacial (C_m) and internal (C_i) water from the measured heat capacity C_p.

untouched for a period of a few days. The wet samples were dried at approximately 383 K in an electric oven. A mass of 2 g of the prepared sample was placed in a sample cell, and water was introduced from the gas phase at a controlled programmed pressure for capillary filling and monolayer adsorption according to the adsorption isotherms shown in Fig. 1. Thus, excess external water was avoided in determining the C_p values accurately. This procedure differs from that employed by Nagoe *et al.*[24] who measured samples with some external bulk water. They estimated the contribution of the external ice by assuming a value of the heat of melting of ice, but did not take into account the special property of boundary water over the porous particle.[10]

The sealed sample cell, whose dead space was filled with helium gas, was mounted in a cryostat. The heat capacity measurements of dried, monolayer, and capillary-filling MCM-41 samples were made while increasing the temperature after first cooling the system to 80 K at a cooling rate of approximately 2 K min^{-1}. The water content of the sample was determined after each heat capacity measurement by weighing the sample cell. For a monolayer system, C10 and C16 samples were tested. After measurements made on several samples for each system, the experimental uncertainties of the obtained values were at most 10%, which was less stable than those for capillary-filling systems. A mean value of several measurements was used in the analysis. These uncertainties bring in about 3% of maximum uncertainty in corrected heat capacity of internal water, C_i, which will be defined in Sec. III.

3. Differential scanning calorimetry

DSC measurements were made on a Q10 calorimeter (TA Instruments, USA) at a scanning speed of 2 K min^{-1}. The melting point could be determined independent of the scanning speed below 7 K min^{-1}.[10] The mass of sample used was approximately 4 mg. Water was introduced from the gas phase up to the capillary filling point for a loosely sealed aluminium sample pan in the gas adsorption system previously described. After adsorption, the sample pan was immediately sealed within a period of 3 min.

4. Inelastic neutron scattering

INS spectra were measured on the time of flight spectrometer LAM-D installed at the pulsed spallation neutron source at the High Energy Acceleration Research Association (KEK). The registered neutron energy was fixed to 4.59 meV using Pyrolytic Graphite 002 reflections. Cooled Be filters were placed in the outgoing beam path to eliminate the higher harmonic neutrons. Powder samples C10 and C18 (~0.5 g) were packed in a cylindrical aluminium cell and exposed to water vapour according to the adsorption isotherms in Fig. 1 in a glass chamber. Monolayer sample C18 was exposed with water vapour at a relative water vapour pressure of 0.2. The sample cell was filled with He gas after the sample was adsorbed with water, and set in a cryostat of a closed cycle He gas refrigerator. First, the samples were cooled down to 50 K during ~3 h and then increased stepwise for measurements. The duration time was 18 h for each sample.

III. RESULTS AND DISCUSSION

A. Heat capacity of water confined in MCM-41

1. Heat capacity of internal water in MCM-41

Figure 2(a) shows the C_p values of capillary filled pore water (abbreviated as pore water) for samples C10–C18 and ML water for sample C16 of MCM-41. Those for ice I_h[29] and bulk liquid water[30] are also shown as a reference. As has been reported in our previous DSC measurements,[10] the interfacial water bound to the pore walls, e.g., monolayer water, is not involved in the freezing and melting in the temperature range measured. Thus, the heat capacity of the interfacial water has to be subtracted from the measured data of the pore water to obtain that of the internal water. This idea is supported by a structural analysis by neutron diffraction.[20] The C_p values of pore water shown in Fig. 2 can be expressed by Eq. (1)

$$C_p = C_i R_i + C_m(1 - R_i), \quad (1)$$

where C_i and C_m are the heat capacity of the internal water and the interfacial water, respectively, and R_i is the molar ratio of the internal water to the pore water. Here, we assumed the values of C_m equal to those of the monolayer water of

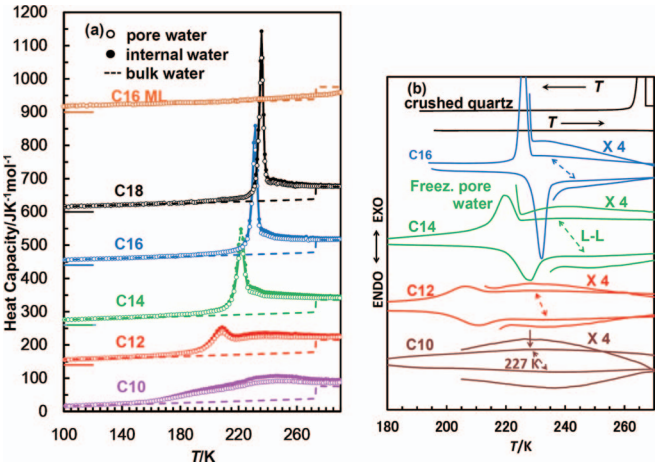

FIG. 2. (a) Temperature change of the heat capacity (open symbols) C_p and C_i (closed symbols) of pore and internal water confined in MCM-41, respectively, and C_p of the monolayer (ML) water adsorbed onto the pore surface of sample C16. The broken lines denote those of bulk water (ice I_h and liquid water). The values of C_i were obtained by assuming that the pore water in the capillary filled state composes of both interfacial and internal water and that the contribution of the interfacial water is equal to that of the monolayer water. (b) DSC curves of water filled in the mesopores of MCM-41 (C12–C16) representing the L–L transitions before and after crystallization and melting of pore water. For sample C10, only L–L transition is detectable. The data of water contacted with crushed quartz without pores are also shown to confirm the stability of the base line of the DSC measurements. The scanning rate was 2 K min^{-1} in the measurements.

sample C16. The amount of the internal water for each MCM-41 system was estimated from a difference between those of capillary filled water and of monolayer water as shown by arrows in the adsorption isotherms (Fig. 1). Since the arrows are placed at appropriate vapour pressures for both monolayer and capillary filling states on the adsorption isotherms, the R_i values might contain estimated uncertainties of about 10%. The heat capacity of the internal water, C_i, was then calculated by Eq. (1). This assumption has been verified by the fact that the heat of melting in the capillary filling range was determined as a function of the amount of adsorbed water, resulting in a constant molar heat of melting. The values of C_i of the internal water are plotted as a function of temperature, together with the measured C_p values. As can be seen in the figure, the values of the internal water are always larger than those for the pore water. The deviations of the values of the internal water from those of bulk water become pronounced with decreasing pore size.

The change in C_p is similar to that reported by Nagoe *et al.*[24] except for the following point. That is, they did not show the C_p values in the temperature range above 255 K for the melting of external water, but those in the temperature range below 255 K which are essentially independent of the pore size in the range of 1.7–2.4 nm. For sample C10, a broad endothermic peak appears at approximately 190 K. This is assigned to the melting of frozen and/or glassy pore water. After this, another broad peak appears at 235–245 K. With increasing pore size, this broad peak tends to overlap with the sharp peak due to melting of pore water and is thus observed as a tail of the high temperature side of the sharp peak for sample C14. For samples C16 and C18, the corresponding peak is completely merged into the sharp peak. The appearance of this peak at almost similar temperature of 235–245 K for C10 and C12 agrees with the observations by Nagoe *et al.*[24] It should be emphasized that this peak appears after the melting of pore water. This finding does suggest that a phase change occurs in the liquid state.

This transition is also clearly detected in the DSC curves of the capillary filled water with lowering and elevating temperature (Fig. 2(b)). For sample C10, corresponding to a broad endothermic peak at 235–245 K in the heating curve, a broad but clear exothermic peak is observed at about 227 K in the cooling curve. Although the temperature of 227 K is slightly lower than those found in previous experiments using neutron scattering,[11,12,31] nuclear magnetic resonance (NMR),[31–34] and FTIR,[13,35,36] the peak has been identified as a phase transition temperature from fragile to strong liquid water. From these findings in the heat capacity and DSC measurements, it is reasonable to ascribe the broad hump at 235–245 K in the C_p curves as the L–L transition of pore water. As can be seen in Fig. 2(a), the value of C_p for monolayer water is close to that of ice I_h in the temperature range below about 240 K and deviates slightly with increasing temperature, but still remains below the value of bulk liquid water.

The C_p values for all the systems merge into that of hexagonal ice at 100 K. With increasing temperature, the C_p values of water confined in small pores, particularly, C10, are larger than the bulk values and does not converge towards the value of bulk water at 290 K.

2. Comparison of C_p change with DSC curves for water in MCM-41

Figure 3(a) shows a comparison between the DSC and C_p values to discuss about a mechanism of the phase change of water in confinement. The thermodynamic melting point is assigned to the peak temperature of the C_p curves. On the other hand, in the DSC data, which are dynamic in nature, the onset temperature of the endothermic peak at the slowest speed can be regarded as the melting point. A clear endothermic peak is not seen for the DSC curve of water in sample C10, while a broad but clear peak is observed at 180–190 K in the C_p curve (see Fig. 2(a)).

Figure 3(b) shows a plot of the melting points determined from the two methods as function of inverse of effective pore size which is obtained by subtraction of thickness t of an interfacial water from the pore size. The value of t has been determined to be 0.39 nm from least-squares fits of the melting points for large pore radii of C16, C18, C22, and SBA-15 according to the G–T relation which is essentially valid when the melting temperature shift by confinement is small.

As can be seen in Fig. 3(a), the melting points from the C_p and DSC curves agree reasonably well with each other for capillary filled water in the largest pores of sample C18, but tend to deviate from each other, accompanied by broadening of the DSC curves, with decreasing pore size. This fact implies that the melting of the frozen water in smaller pores, such as C10 and C12, does not take place in a single process, but in a multiple step for heterogeneous fine crystallites in confinement. The melting point determined from the C_p data

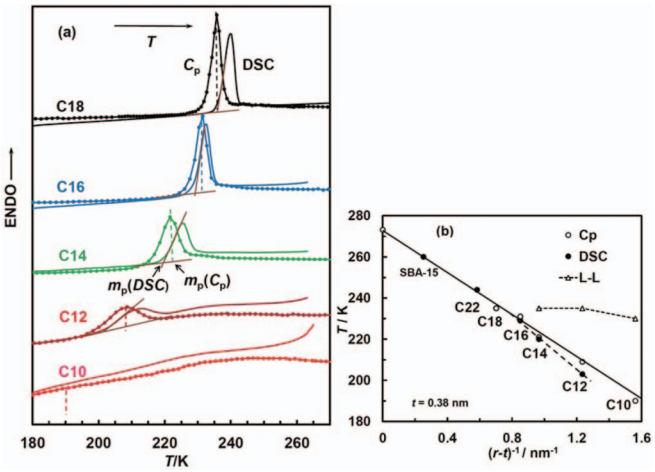

FIG. 3. (a) A comparison of the C_p curve (lines with symbols) and the DSC curve (solid lines) in the warming direction of water confined in MCM-41. Both values were arbitrarily magnified to make the comparison clear. The DSC curves were measured at a heating rate of 2 K min^{-1}. The onset temperature does not vary when the scanning rate was below 7 K min^{-1}. The melting point, m_p (DSC), was designated at a crossing point between the base line and the tangential line on the left-hand side of the peak, i.e., onset temperature of melting. The value of melting point, $m_p(C_p)$, was determined as the peak position of the C_p curves. (b) Plots of the melting point of water determined from the C_p and DSC measurements as a function of the inverse of the effective pore radius. The melting point of samples C22 and SBA-15 are added from a previous work.[10] The terms r and t denote the pore radius and the thickness of interfacial water (0.38 nm), respectively.

follows well an inverse linear relationship with the effective pore size, i.e., $(r-0.38)^{-1}$. The peak temperature of the broad C_p curve of sample C10 at 190–200 K (Fig. 2) falls almost at the limit of this line, and it is reasonable to suppose that the frozen and/or glassy water in sample C10 gradually melts at a temperature of around 187 K, followed by the L–L transition at 235 K.

3. Entropy of water in MCM-41

Thermodynamically, the entropy of pore water provides more direct information on the state of the water in confinement. The entropy of pore water can be expressed by Eq. (2)[37]

$$S = S_0 + \int_0^T \frac{C_i}{T} dT + \Delta S_{tr}, \quad (2)$$

where S_0 is the residual entropy at 0 K. For crystalline ice, this value is 3.41 J K^{-1} mol^{-1},[38] which arises from the fact that the position of proton in a hydrogen bond between the neighbouring oxygen atoms of water molecules is not decisively assigned. The structure of water frozen in the pores such as C10 is probably deformed from the perfect ice structure, thus the position of protons is less well defined than that in the crystalline ice, resulting that the value of S_0 should be higher than that of bulk ice. However, so far, no S_0 values for confined water are available in the literature. The term ΔS_{tr} denotes a change in entropy for phase transition taking place between 0 and T K. In the present system, this term is included in the integration term and was neglected because the phase transition is gradual.

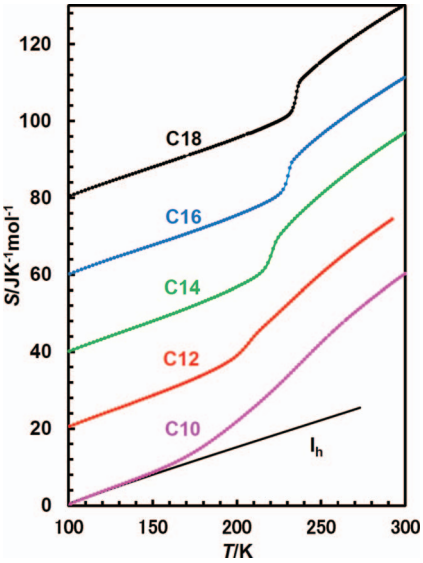

FIG. 4. Entropy values estimated from the C_i values of the internal water confined in MCM-41, where the starting value was fixed arbitrarily on the ordinate since the residual entropy of the confined water in the mesopores of MCM-41 is available. The line in black is for Ih.

Figure 4 shows a change in entropy of the internal water confined in MCM-41, where the entropy values were obtained from the C_i values measured as a function of temperature as discussed in Sec. III A 2. Here, the starting value used to calculate the entropy was arbitrarily on the ordinate.

For the water in sample C10, the entropy values increase steeply with temperature, compared with that of bulk ice, and reach a value which is much higher than that of bulk water. The increase in the entropy values for samples C12–C18 is moderate, but still steeper than that of ice I_h. This pore size dependence of entropy change is ascribed to the structural and dynamic properties of frozen or deeply supercooled water which should be related to the density of these phases. Bertrand *et al.*[39] reviewed the density of water confined in MCM-41 with temperature to focus a density minimum of the confined water in small pores. The minimum density of H_2O in confinement is 0.9412 g cm^{-3}, which is scaled by 10.6% from 1.041 g cm^{-3} for D_2O obtained by small-angle neutron scattering (SANS) measurements. The minimum density temperature is 190 K for H_2O from small-angle X-ray scattering (SAXS) and 210 K for D_2O from SANS. This temperature range corresponds to a broad peak at around 190 K for the C_p curve of C10, where LDL exists in the pore. This assignment of LDL is also verified from the fact that the minimum density of 0.9412 g cm^{-3} is in good agreement with the density (0.94 g cm^{-3}) of H_2O low-density amorphous (LDA) ice. Erko *et al.*[40] reported the effect of pore size (diameter = 2.0, 3.4, 3.9, and 4.4 nm) on the density minimum from comparative SAXS and SANS measurements. For the larger pores, they attributed the density minimum to a liquid-solid transition of water influenced by confinement. On the other hand, for the smallest pore of 2.0 nm, they claimed that the density minimum is explained in terms of a structural transition of the surface water layer closest to the hydrophilic pore walls since

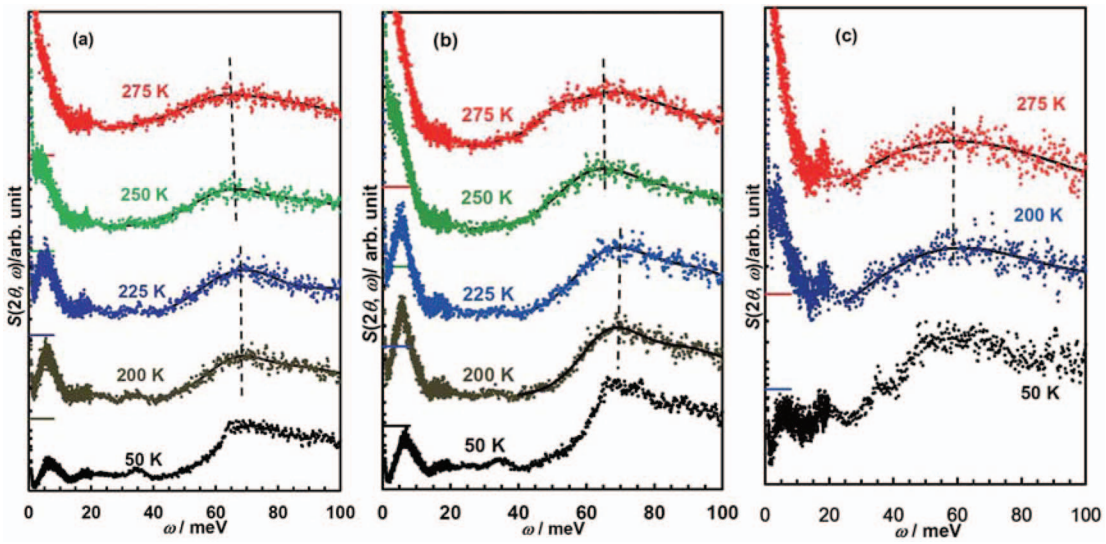

FIG. 5. Temperature dependence of the INS spectra of water confined in MCM-41: (a) sample C10, (b) C18, and (c) in the monolayer water adsorbed on the pore surface of C18. The solid lines were estimated by fitting 2 or 3 Gaussian functions using the fitting program ORIGIN (Microcal, USA). The dashed lines are drawn to clarify the change in peak position with temperature.

the fraction of surface water within the pore of 2.0 nm size is around 84%. However, in our C_p analysis mentioned previously for MCM-41 C10, the fraction of the internal water, R_i, is experimentally determined to be 0.75, and thus the behaviour of the C_p curve for C10 is due to the internal water, not to the interfacial water.

As can be seen in Fig. 4, there are steps in the entropy curves at the temperature corresponding to the melting region of frozen water. According to the data from quasi-elastic neutron scattering measurements,[41,42] the translational motion of water confined in such a small pore as C10 is hindered strongly, whereas the rotational motion is similar to that of bulk water. Thus, the larger entropy values for water confined in the small pores are ascribed to an increased structural deformation.[43]

4. INS of water confined in MCM-41

As has been reported in a previous work of quasi-elastic neutron scattering measurements,[41] the confinement of water molecules significantly decreases the translational diffusion coefficient with a decrease in pore size. Molecular vibration of water observed by FTIR measurements is strongly affected by confinement: the OH stretching band becomes less sharp by confinement for small pores, such as C10.[10] This suggests deformation of hydrogen bonds among water molecules in confinement.

INS gives direct information on the strength of hydrogen bonds formed between water molecules and/or its domains. Figure 5(a) shows the INS spectra of capillary filled water in C10 as a function of temperature. The spectra are mainly composed of two modes of motion of water molecule: a hindered translational motion at 7–35 meV and a librational one at ~65 meV. Liu *et al.*[31] measured the INS spectra on water confined in MCM-41-S-15 (pore size 1.8 nm), but did not observe the peaks of the hindered translation in a low energy region. They reported an increment of the spectra for the librational motion of 50 meV at 220–230 K and ascribed it to the L–L transition. As can be seen in Fig. 5(a) in the present study, a small discontinuous shift and broadening of spectra are evident between 225 and 250 K. In the energy range of translational motion, the peaks at l8 and 35 meV are markedly weakened. This fact suggests the destruction of long-range ordering of water molecules.[44] Furthermore, the peak for the hindered translation tends to merge with the evolved peak of quasi-elastic neutron scattering. In the case of C18 system (Fig. 5(b)), the peak for the librational motion changes discontinuously at 225–250 K with increasing temperature; this corresponds to the melting of frozen water.

According to the data from the calorimetric measurements previously discussed, the structure of frozen water in confinement is very different from that of bulk ice. Here, we compare the vibrational mode of confined water observed by INS with those of bulk frozen water (crystalline, amorphous, and heated amorphous ices). Figure 6(a) shows the INS spectra of bulk water in different forms measured at 50 K by Yamamuro *et al.*[45] Figure 6(b) shows the INS spectra for

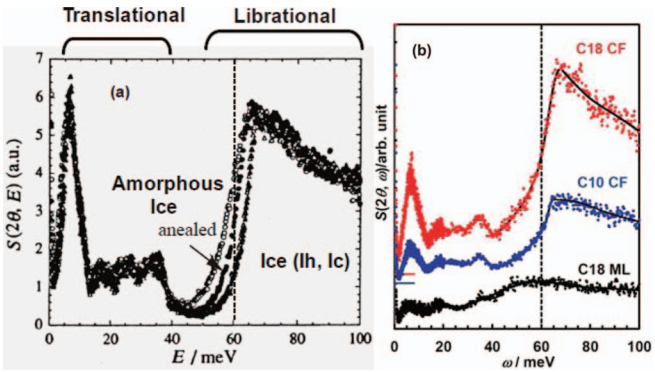

FIG. 6. INS spectra of ice: (a) amorphous, I_h, and I_c,[45] and (b) water capillary-filled in samples C10 and C18, and the monolayer water adsorbed on the pore surface of C18. The spectra are displaced upward arbitrarily for clarity.

monolayer water in C18 and pore water in C10 and C18. In the cases of pore water, the spectra differ largely in intensity between C10 and C18 due to the different amounts of water adsorbed in the two systems, but the magnification of the spectrum for C10 by 2.4 times resulted in an indistinguishably similar feature to C18 (see the supplementary material[50] for INS magnification). The edge energy of the librational motion of both samples indicated by dashed lines is very similar to that for amorphous ice in Fig. 6(a).

Figure 6(b) shows the spectrum of the monolayer water adsorbed on the pore surface of sample C18. Besides lowering in intensity because of much less water adsorbed, the spectrum shows a broadened librational band whose edge in the lower energy side is extended to above 30 meV, i.e., to a smaller vibration energy. The band below 30 meV is very small and does not change with temperature. This fact suggests that the monolayer water lacks in hydrogen bonds between water molecules. In the case of water on the silica surface, the monolayer water is probably not smoothly spread over the surface even after hydration, but localized to the surface hydroxyls to form patches by strong hydrogen bonding. This explains why the spectrum broadens with increasing temperature, but much less markedly than the capillary filled water. Furthermore, this is substantiated from the C_p measurements in Fig. 2 and neutron spin echo measurements on monolayer water adsorbed on the pore surface of sample C10.[46] The structural rigidity of the interfacial water in the presence of capillary condensed internal water is also confirmed by the neutron diffraction analyses.[20] The comparatively small contribution of translational diffusion reported by Liu *et al.*[31] might be explained by a larger amount of monolayer water due to a smaller pore size (1.8 nm) than that of the present sample (2.1 nm).

5. Observation of L–L transition

There are many experimental reports for the L–L transition by using various techniques for water in confinement.[11–13,31–36] To our knowledge, however, there seems no rationale on a mechanism of this transition. The idea of the L–L transition stems from a model for bulk water proposed by Mishima and Stanley[47] on the basis of their computer simulation study. Since bulk water is frozen below the homogeneous nucleation temperature (HNT) of 235 K, it is impossible to look into the behaviour of supercooled water below HNT. As it has been experimentally established that there are two forms of amorphous ice: low density amorphous (LDA) and high density amorphous (HDA) ones,[44] it is rational to postulate the corresponding molten forms (LDL and HDL water) above an upper limit of temperature of the amorphous phases, the so-called no-man's land.[47] The liquid water below HNT can be prepared in small mesopores of silica where due to the larger interfacial free energy of the first layer water of silica wall, compared with the energy of the internal water, the freezing and melting points are lowered according to the Gibbs–Thomson relation. In fact, when the pore size is below ~2.1 nm, the pore water is not frozen to form crystalline ice. Thus, a large number of studies on the properties of low-temperature confined water below HNT have been carried out by using various methods.

Along with this context, there is an intention to extrapolate the experimental results obtained for confined water to phenomena of bulk water in the no man's land.[47] Apparently, the L–L transition temperature obtained for confined water falls on the Widom line which is a calculated L–L equilibrium line extended from the postulated 2nd critical point of water.[31] It should be kept in mind, however, that the L–L transition is observed only on water confined in mesopores, e.g., MCM-41 and hydrated proteins,[48] whose pore size might be below 2.1 nm or so as discussed above. The L–L transition is observed at a temperature close to HNT, and thus seems to occur gradually as found in the experiments by NMR,[33] FTIR,[36] and the present calorimetry. In the case of inelastic neutron scattering measurements on the dynamics of confined water, the relaxation time increases gradually and follows the VFT function and suddenly changes to an Arrhenius type at the transition temperature.[11,12] There are no stepwise jumps in the dynamic properties of confined water at the transition temperature. In other word, we might say that the internal water below HNT and above ~190 K is structured due to reinforced hydrogen bonds and of low density like ice without crystallization due to the confinement effect.

When water is cooled, the density of liquid water decreases gradually after passing the maximum at 278 K and does markedly at HNT.[35] In the cooling process, water molecules probably form a number of clusters which are fragile to decompose and reform. This would be a picture of fragile water, or high density liquid water.

Matsumoto *et al.*[49] studied the dynamic process of crystallization of water below HNT at the molecular level by MD simulation using a TIP4P model and found that there are some stages of clustering of water molecules to reach crystallization of water. After an induction period (stage 1), the homogeneous nucleation of ice starts, (stage 2) 5, 6, and 7 membered clusters of water begin to form 6-membered ones whose bonds are long-lived and form a network of rather opened structure, and (stage 3) reaches the state to grow more ordered compact network, but a frustrated system with collective motions, i.e., low density liquid. Finally, they grow as crystalline ice very quickly (stage 4). They calculated the corresponding potential energy of the system and found that it decreases, reflecting the growth of hydrogen bonds. On the basis of a decrease in the O–H vibrational energy of confined water obtained in our previous FTIR study,[10] together with the above-mentioned MD results, different behaviours of enthalpy change of water confined with pore size are discussed here.

Figure 7(a) shows schemes of enthalpy changes of water confined in (1) large mesopore (e.g., C18), (2) medium one (e.g., C14), and (3) small one (e.g., C10). As the temperature is decreased, the enthalpy of water in large pores decreases until the water freezes at temperature "b" according to the G–T relation. In the case of water in medium mesopores, the enthalpy of confined water gradually decreases due to the growth of hydrogen bonding to form low density water at temperature "c" and follow line 2 to reach temperature "d" where the water freezes to ice as controlled by the G–T relation.

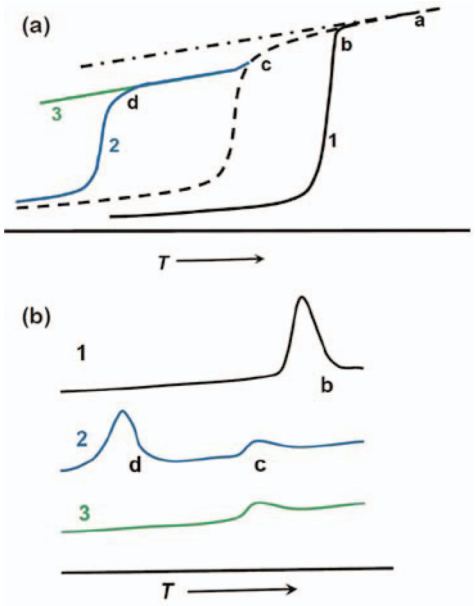

FIG. 7. Scheme of (a) enthalpy and (b) C_p changes of confined water with temperature in the region of the phase changes. Line number 1 is for water in mesopores presenting freezing temperature higher than HNT (e.g., C18); the enthalpy change for homogeneous nucleation crystallization is shown by a broken line. Line number 2 is for water confined obeying the G–T relation (e.g., C12). Line 3 is for water which does not crystallize until very low temperature at around 190 K (C10).

Water in small pores is kept unfrozen down to a much lower temperature (line 3). The derivatives of the enthalpy curves in Fig. 7(b) show the corresponding behaviour of C_p values for these systems as shown in Fig. 1(a). Thus, we can conclude that the L–L transition so far named is a transformation of homogeneous nucleation-like structuring from ordinary fragile water (HDL) to hexagonal network clusters (LDL) whose density is lower than that of HDL without crystallization to ice.

IV. CONCLUSIONS

The phase properties of the liquid and solid states of pore water confined in MCM-41 were studied by measuring the heat capacity and INS spectra. The value of the entropy of the confined water was estimated from the heat capacity of internal water derived from the C_p values. It increases rapidly than that of bulk ice. This effect becomes significant for smaller pores, reflecting the deformation of structure of confined water. Hydrogen bonding between water molecules differs from that in crystalline ice, even at 50 K, representing an amorphous nature for water frozen in the pores. This observation makes us anticipate that the residual entropy of the pore water at 0 K would be augmented from that of bulk crystalline ice. The L–L transition so far discussed as the first order transition for water confined in small mesopores is explained by the freezing of low density liquid state of water prior to crystallization at HNT. This phase is formed in the mesopores when the freezing temperature is below HNT. When the frozen phase is warmed, it appears again just after melting. The hump observed in the C_p measurements around 235–240 K is attributed to the easing of LDL to fragile HDL water.

ACKNOWLEDGMENTS

This work was partly supported by Grant in Aid for Science Research No. 15750015 from the Ministry of Education Science and Culture of Japan and by a Special Grant for Cooperative Research administered by the Japan Private School Promotion Foundation.

[1]T. Yanagisawa, T. Shimizu, K. Kuroda, and C. Kato, Bull. Chem. Soc. Jpn. **63**, 988 (1990).
[2]C. T. Kresge, M. E. Leonowicz, W. J. Roth, J. C. Vartuli, and J. S. Beck, Nature (London) **359**, 710 (1992).
[3]K. Schumacher, P. I. Ravikovitch, A. Du DChesne, A. V. Neimark, and K. K. Unger, Langmuir **16**, 4648 (2000).
[4]D. Y. Zhao, J. L. Feng, Q. S. Huo, N. Melosh, G. H. Fredrickson, B. F. Chmelka, and G. D. Stucky, Science **279**, 548 (1998).
[5]D. Y. Zhao, Q. S. Huo, J. L. Feng, B. F. Chmelka, and G. D. Stucky, J. Am. Chem. Soc. **120**, 6024 (1998).
[6]F. Kleitz, D. Liu, G. M. Anikumar, I.-S. Park, I. A. Solovyov, A. N. Shmakov, and R. Ryoo, J. Phys. Chem. B **107**, 14296 (2003).
[7]C. Yu, Y. Yu, and D. Zhao, Chem. Commun. **2000**, 575.
[8]A. Schreiber, I. Ketelsen, and G. H. Findenegg, Phys. Chem. Chem. Phys. **3**, 1185 (2001).
[9]K. Morishige and K. Kawano, J. Chem. Phys. **110**, 4867 (1999).
[10]S. Kittaka, S. Ishimaru, M. Kuranishi, T. Matsuda, and T. Yamaguchi, Phys. Chem. Chem. Phys. **8**, 3223 (2006).
[11]A. Faraone, Li Liu, C.-Y. Mou, C.-W. Yen, and S.-H. Chen, J. Chem. Phys. **121**, 10843 (2004).
[12]K. Yoshida, T. Yamaguchi, S. Kittaka, M.-C. Bellissent-Funel, and P. Fouquet, J. Chem. Phys. **129**, 054702 (2008).
[13]S. Kittaka, K. Sou, T. Yamaguchi, and K. Tozaki, Phys. Chem. Chem. Phys. **11**, 8538 (2009).
[14]S. Kittaka, Y. Ueda, F. Fujisaki, T. Iiyama, and T. Yamaguchi, Phys. Chem. Chem. Phys. **13**, 17222 (2011).
[15]J. Seyed-Yazdi, H. Farman, J. C. Dore, J. B. Webber, G. H. Findenegg, and T. Hansen, J. Phys. Condens. Matter **20**, 205107 (2008).
[16]E. Liu, J. C. Dore, J. B. Webber, D. Khushalani, S. Jähnert, G. H. Findenegg, and T. Hansen, J. Phys. Condens. Matter **18**, 10009 (2006).
[17]K. Morishige and H. Uematsu, J. Chem. Phys. **122**, 044711 (2005).
[18]E. B. Moore, E. de la Llave, K. Welke, D. A. Scherlis, and V. Molinero, Phys. Chem. Chem. Phys. **12**, 4124 (2010).
[19]E. B. Moore and V. Molinero, Phys. Chem. Chem. Phys. **13**, 20008 (2011).
[20]R. Mancinelli, F. Bruni, and M. A. Ricci, J. Phys. Chem. Lett. **1**, 1277 (2010).
[21]P. Johari, J. Chem. Phys. **130**, 124518 (2009).
[22]E. Tombari, G. Salvetti, C. Ferrari, and G. P. Johari, J. Chem. Phys. **122**, 104712 (2005).
[23]M. Oguni, Y. Kanke, A. Nagoe, and S. Namba, J. Phys. Chem. B **115**, 14023 (2011).
[24]A. Nagoe, Y. Kanke, M. Oguni, and S. Namba, J. Phys. Chem. B **114**, 13940 (2010).
[25]K. L. Ngai, S. Capaccioli, M. S. Thayyil, and N. Shinyashiki, J. Therm. Anal. Calorim. **99**, 123 (2010).
[26]T. Mori, Y. Kuroda, Y. Yoshikawa, M. Nagao, and S. Kittaka, Langmuir **18**, 1595 (2002).
[27]D. Dollimore and G. R. Heal, J. Appl. Chem. **14**, 109 (1964).
[28]K. Moriya, T. Matsuo, and H. Suga, J. Chem. Thermodyn. **14**, 1143 (1982).
[29]O. Haida, T. Matsuo, H. Suga, and S. Seki, J. Chem. Thermodyn. **6**, 815 (1974).
[30]*Water: A Comprehensive Treatise*, edited by F. Franks (Plenum Press, 1982), Vol. 7.
[31]L. Liu, S.-H. Chen, A. Faraone, C.-W. Yen, C.-Y. Mou, A. I. Kolesnikov, E. Mamontov, and J. Leao, J. Phys. Condens. Matter **18**, S2261 (2006).
[32]F. Mallamace, M. Broccio, C. Corsaro, A. Faraone, D. Majolino, V. Venuti, L. Liu, C.-Y. Mou, and S.-H. Chen, J. Phys. Condens. Matter **18**, S2285 (2006).
[33]F. Mallamace, M. Broccio, C. Corsaro, A. Faraone, U. Wanderlingh, L. Liu, C.-Y. Mou, and S. H. Chen, J. Chem. Phys. **124**, 161102 (2006).

[34]F. Mallamace, C. Corsaro, M. Broccio, C. Branca, N. Gonzalez-Segredo, J. Spooren, S.-H. Chen, and H. E. Stanley, Proc. Natl. Acad. Sci. U.S.A. **105**, 12725 (2008).
[35]F. Mallamace, C. Branca, M. Broccio, C. Corsaro, C.-Y. Mou, and S.-H. Chen, Proc. Natl. Acad. Sci. U.S.A. **104**, 18387 (2007).
[36]F. Mallamace, M. Broccio, C. Corsaro, A. Faraone, D. Majolino, V. Venuti, L. Liu, C.-Y. Mou, and S.-H. Chen, Proc. Natl. Acad. Sci. U.S.A. **104**, 424 (2007).
[37]D. Eisenberg and W. Kauzmann, *The Structure and Properties of Water* (Clarendon Press, London, 1969).
[38]H. Savage, *Water Structure in Crystalline Solids*, Water Science Reviews Vol. 2, edited by F. Franks (Cambridge University Press, Cambridge, 1986).
[39]C. E. Bertrand, Y. Zhang, and S. H. Chen, Phys. Chem. Chem. Phys. **15**, 721 (2013).
[40]M. Erko, D. Wallacher, A. Hoell, T. Hauss, I. Zizak, and O. Paris, Phys. Chem. Chem. Phys. **14**, 3852 (2012).
[41]S. Takahara, M. Nakano, S. Kittaka, Y. Kuroda, T. Mori, H. Hamano and T. Yamaguchi, J. Phys. Chem. **103**, 5814 (1999).
[42]S. Takahara, N. Sumiyama, S. Kittaka, T. Yamaguchi, and M.-C. Bellissent-Funel, J. Phys. Chem. B **109**, 11231 (2005).
[43]P. Smirnov, T. Yamaguchi, S. Kittaka, S. Takahara, and Y. Kuroda, J. Phys. Chem. B **104**, 5498 (2000).
[44]A. I. Kolesnikov, J. Li, S. F. Parker, R. S. Eccleston, and C.-K. Loong, Phys. Rev. B **59**, 3569 (1999).
[45]O. Yamamuro, Y. Madokoro, H. Yamasaki, T. Matsuo, I. Tsukushi, and K. Takeda, J. Chem. Phys. **115**, 9808 (2001).
[46]K. Yoshida, T. Yamaguchi, S. Kittaka, M.-C. Bellissent-Funel, and P. Fouquet, J. Phys. Condens. Matter **24**, 064101 (2012).
[47]O. Mishima and H. E. Stanley, Nature (London) **396**, 329 (1998).
[48]F. Mallamace, C. Corsaro, P. Baglioni, E. Fratini, and S.-H. Chen, J. Phys. Condens. Matter **24**, 064103 (2012).
[49]M. Matsumoto, S. Saito, and I. Ohmine, Nature (London) **416**, 409 (2002).
[50]See supplementary material at http://dx.doi.org/10.1063/1.4807593 for (a) pore size distributions and (b) INS magnification.